The American Journal of Pathology, Vol. 184, No. 5, May 2014

ELSEVIER

The American Journal of PATHOLOGY

ajp.amjpathol.org

VASCULAR BIOLOGY, ATHEROSCLEROSIS, AND ENDOTHELIUM BIOLOGY

# Ceramide-Activated Phosphatase Mediates Fatty Acid–Induced Endothelial VEGF Resistance and Impaired Angiogenesis

Vishal C. Mehra,[*†‡] Elias Jackson,[*†‡] Xian M. Zhang,[*] Xian-Cheng Jiang,[§] Lawrence W. Dobrucki,[*] Jun Yu,[¶] Pascal Bernatchez,[¶] Albert J. Sinusas,[*] Gerald I. Shulman,[*‖] William C. Sessa,[¶] Timur O. Yarovinsky,[*†‡] and Jeffrey R. Bender[*†‡]

*From the Departments of Internal Medicine,* Immunobiology,† and Pharmacology¶, the Raymond and Beverly Sackler Foundation Cardiovascular Laboratory,‡ and the Howard Hughes Medical Institute,‖ Yale Cardiovascular Research Center, Yale University School of Medicine, New Haven, Connecticut; and the SUNY Downstate Medical Center,§ Brooklyn, New York*

Accepted for publication January 2, 2014.

Address correspondence to Jeffrey R. Bender, M.D., YCVRC, Yale School of Medicine, 300 George St, New Haven, CT 06511. E-mail: jeffrey.bender@yale.edu.

Endothelial dysfunction, including endothelial hyporesponsiveness to prototypical angiogenic growth factors and eNOS agonists, underlies vascular pathology in many dysmetabolic states. We investigated effects of a saturated free fatty acid, palmitic acid (PA), on endothelial cell responses to VEGF. PA-pretreated endothelial cells had markedly diminished Akt, eNOS, and ERK activation responses to VEGF, despite normal VEGFR2 phosphorylation. PA inhibited VEGF-induced angiogenic cord formation in Matrigel, and PA-treated endothelial cells accumulated early species (C16) ceramide. The serine palmitoyltransferase inhibitor myriocin reversed these defects. Protein phosphatase 2A (PP2A) became more eNOS-associated in PA-treated cells; the PP2A inhibitor okadaic acid reversed PA-induced signaling defects. Mice fed a diet high in saturated fat for 2 to 3 weeks had impaired i) aortic Akt and eNOS phosphorylation to infused VEGF, ii) ear angiogenic responses to intradermal adenoviral-VEGF injection, and iii) vascular flow recovery to hindlimb ischemia as indicated by laser Doppler and $\alpha_v\beta_3$ SPECT imaging. High-fat feeding did not impair VEGF-induced signaling or angiogenic responses in mice with reduced serine palmitoyltransferase expression. Thus, *de novo* ceramide synthesis is required for these detrimental PA effects. The findings demonstrate an endothelial VEGF resistance mechanism conferred by PA, which comprises ceramide-induced, PP2A-mediated dephosphorylation of critical activation sites on enzymes central to vascular homeostasis and angiogenesis. This study defines potential molecular targets for preservation of endothelial function in metabolic syndrome. *(Am J Pathol 2014, 184: 1562–1576; http://dx.doi.org/10.1016/j.ajpath.2014.01.009)*

Endothelial dysfunction is the inability of the endothelium to promote vasodilation in a stimulus-dependent fashion, primarily as a consequence of impaired nitric oxide (NO) production. Individuals with risk factors for vascular disease, including metabolic syndrome and dysplipidemia,[1] exhibit varying degrees of endothelial dysfunction, which is an early feature of vascular pathology with prognostic significance.[2] Elevation of circulating free fatty acids (FFAs), experimentally or as seen in obese insulin-resistant individuals and in type 2 diabetes, results in 40% to 50% lower endothelium-dependent vasodilation.[3,4] The elevation of circulating FFA in obesity, metabolic syndrome, and type 2 diabetes is associated with impaired endothelium-dependent vasodilation, suggesting a link between FFA and endothelial dysfunction. We investigated such a link by assessing the effect of FFA on NO-producing growth factor signaling in the endothelium.

Similar to hyperinsulinemia in insulin resistance, elevated systemic VEGF levels have been detected in individuals with visceral obesity, type 2 diabetes, and atherosclerosis.[5,6] VEGF levels are also elevated in chronically ischemic

Supported by NIH grants R01-HL061782 (J.R.B.), T32-HL007950 (V.C.M.), R01-DK400936 (J.S.), and the Raymond and Beverly Sackler Foundation.

Disclosures: GE Healthcare provided the SPECT imaging agent.

Current address of V.C.M., Johns Hopkins Medicine, Baltimore, MD, and the National Heart, Lung and Blood Institute, NIH, Bethesda, MD; of E.J., School of Medicine, American University of Antigua, Antigua.


http://dx.doi.org/10.1016/j.ajpath.2014.01.009

coronary and peripheral artery disease states,[6] as well as in essential hypertension.[7] In the present study, we evaluated the effects of palmitic acid (PA) on endothelial signaling responses to VEGF. PA profoundly impaired VEGF-dependent eNOS activation and angiogenic responses *in vitro* and in two independent *in vivo* murine models. The effects of PA were dependent on *de novo* synthesis of ceramide, which increased association of protein phosphatase 2A (PP2A) with eNOS. Here, we discuss this VEGF resistance as a possible central feature of the widespread vascular pathology seen in numerous dysmetabolic states.

## Materials and Methods

### Reagents and Cells

Recombinant human VEGF-$A_{165}$ was obtained from the Biological Resource Branch of the National Cancer Institute (Frederick, MD). Sodium palmitate, C2 ceramide, myriocin, okadaic acid (OkA), and bradykinin were obtained from Sigma-Aldrich (St. Louis, MO). Antibodies to bovine eNOS and p-eNOS were from Life Technologies (Zymed brand; Carlsbad, CA), antibodies to mouse eNOS were from BD Biosciences (San Jose, CA), and antibodies to ERK1/2, p-ERK1/2, Akt, p-Akt, and VEGFR2 were from Cell Signaling Technology (Danvers, MA). Antibody to PP2A was from EMD Millipore (Billerica, MA). Primary bovine aortic endothelial cells (BAECs) were purchased from Lonza (Walkersville, MD) and cultured in Dulbecco's modified Eagle's medium (Life Technologies) supplemented with 10% fetal bovine serum (Atlanta Biologicals, Flowery Branch, GA), 100 U/mL penicillin, 100 μg/mL streptomycin, and 2 mmol/L L-glutamine (Life Technologies) and were used up to passage 8. Human umbilical vein endothelial cells (HUVECs) from the Yale Vascular Biology Cell Culture Core Facility were cultured in medium 199 supplemented with 20% fetal bovine serum, 100 U/mL penicillin, 100 μg/mL streptomycin, and EC growth supplement (BD Biosciences) and were used up to passage 6. Fatty acids were conjugated to bovine serum albumin before use by dissolving in 50% ethanol–PBS. The solubilized fatty acid solution was gently added dropwise into 1% essentially fatty acid–free bovine serum albumin (BSA) solution at 45°C. Conjugation of the FFAs to BSA (molar ratio 2:1) was allowed to continue for at least 1 hour at 37°C. Vehicle control for fatty acids constituted equivalent amounts of ethanol and BSA without the fatty acids, and with final ethanol concentrations never exceeding 0.1% (v/v). Similarly, dimethyl sulfoxide at or below 0.1% (v/v) was used as vehicle control for some inhibitors. Cell culture experiments were routinely performed after 16 to 24 hours of serum starvation of the cells in serum-free culture medium containing 0.1% essentially fatty acid–free BSA, unless otherwise noted.

### Animal Models of High-Fat Feeding

All studies with animals were conducted according to a protocol approved by the Yale University Institutional Animal Care and Use Committee. C57BL/6J and AKR/J mice were purchased from the Jackson Laboratory (Bar Harbor, ME). Mice heterozygous for the serine palmitoyltransferase, long chain base subunit 2 gene (*Sptlc2*$^{-/+}$ mice) were backcrossed to C57BL/6J mice for at least six generations and were maintained under specific pathogen–free conditions. These mice express reduced levels of serine palmitoyl-coenzyme A (CoA) transferase, a rate-limiting enzyme in sphingolipid biosynthesis.[8] Wild-type littermates (*Sptlc2*$^{+/+}$) were used as controls for *Sptlc2*$^{-/+}$ mice. To elevate plasma FFA levels, 9- to 12-week-old mice were fed *ad libitum* a 60% fat-based calorie diet (D12492; Research Diets, New Brunswick, NJ) for 17 to 18 days (2.5 weeks). The FFA content of the high-fat diet was as follows (in g/4057 kcal): myristic acid, 2.2; myristoleic acid, 1.2; PA, 58.7; palmitoleic acid, 9.3; stearic acid, 33.5; oleic acid, 106.8; linoleic acid, 34.4; linolenic acid, 4.4; and arachidonic acid, 4.2. Control animals were maintained on normal mouse chow. Plasma FFA levels were measured by an acyl-CoA oxidase-based colorimetric assay [NEFA-HR(2); Wako Diagnostics, Richmond, VA] as described previously.[9]

### VEGF-Induced Aortic Kinase Activation *in Vivo*

Recombinant human VEGF-$A_{165}$ or saline control was infused via a left jugular vein catheter into anesthetized mice fed normal chow (control) or a high-fat diet. After 5 minutes, animals were perfused with phosphatase inhibitors [1 mmol/L sodium orthovanadate ($Na_3VO_4$), 20 mmol/L NaF, and 1 mmol/L sodium pyrophosphate ($Na_4P_2O_7$)], after which the mice were sacrificed and aortas were harvested and immediately flash frozen. Aortic tissue was then homogenized in lysis buffer; after protein quantification, tissue extracts were immunoblotted for p-eNOS, p-Akt, total eNOS, and total Akt.

### Adenoviral VEGF-Driven Ear Angiogenesis

AKR/J white mice were fed a high-fat diet or a control diet (normal chow) and received intradermal injection of recombinant adenoviruses ($1 \times 10^8$ plaque-forming units) encoding murine VEGF-A164 (AdVEGF) into the left ear or control Cre recombinase (AdCre) into the right ear. After 5 days, ears were photographed and then removed from euthanized mice. Fixed cryosections (7 μm thick) were immunostained with monoclonal rat anti-mouse CD31 antibody (BD Biosciences) and Alexa Fluor 488–conjugated anti-rat IgG antibody (Life Technologies). Fluorescent images were obtained on a Zeiss Axioskop microscope (Carl Zeiss Microscopy, Jena, Germany), and CD31-positive staining was quantified with ImageJ software version 1.42a (NIH, Bethesda, MD).

### Hindlimb Ischemia and Laser Doppler Imaging

To induce ischemia, in both control mice and in mice fed a high-fat diet, the femoral artery and vein were ligated just below the inguinal ligament at the level of entry into the

thigh and at the level of the popliteal artery. The intervening segment was excised, and other branches of the femoral artery (including the profunda and the superficial and deep femoral branches) were cauterized. Laser Doppler imaging for blood-flow analysis was performed by placing the Doppler probe directly on the gastrocnemius muscle at 3 days, 1 week, and 3 weeks. Data are expressed as a ratio of flow in the ischemic hindlimb to flow in the nonischemic control (contralateral) hindlimb.

### Matrigel *in Vitro* Cord Formation

HUVECs at passage 4 ($5 \times 10^5$ cells) were suspended in growth factor–reduced Matrigel (BD Biosciences) containing medium with or without various growth factors, fatty acids, and inhibitors. Cells were incubated for 12 to 16 hours at 37°C, after which cord area, length, and branch points were quantified using Metamorph software version 7.1 (Molecular Devices, Sunnyvale, CA) as described previously.[10]

### NO Chemiluminescence

Confluent BAECs were treated with solvent control, PA, or C2 ceramide in serum-free medium for 4 hours. The medium was changed, and after 30 minutes of incubation in fresh medium the supernatants were collected as a prestimulation sample. VEGF-containing medium was then added, and after 45 minutes of incubation the supernatants were collected as a poststimulation sample. Levels of $NO_x$ (defined as $NO_2^-$, $NO_3^-$, and nitrosothiols) were determined by NO-specific chemiluminescence as described previously.[11] In brief, cells were lysed, total protein was quantified, and $NO_x$ levels were normalized to total protein.

### Immunoblotting and Immunoprecipitation

BAECs treated with solvent control, PA, or C2 ceramide were treated with VEGF (or bradykinin), and lysates generated in radioimmunoprecipitation assay buffer were subjected to immunoblotting as described previously.[12] For VEGFR2 immunoprecipitation and for coimmunoprecipitation, treated BAECs were lysed in 50 mmol/L Tris-HCl (pH 7.4), 5 mmol/L $Na_4P_2O_7$, 50 mmol/L NaF, 1 mmol/L $Na_3VO_4$, 1 mmol/L dithiothreitol, 0.5% NP-40, and complete protease inhibitor (cOmplete; Roche Diagnostics, Indianapolis, IN). Experimental molecules (VEGFR2, eNOS, and PP2A) were immunoprecipitated overnight with excess antibody; eluted immunoprecipitates were resolved by SDS-PAGE, then subjected to immunoblotting as described previously.[12] The anti–phosphorylated amino acid antibody specificities were eNOS-$Ser^{1179}$, Akt-$Ser^{473}$, ERK1-$Thr^{202}$/ERK2-$Tyr^{204}$.

### Ceramide Quantification

Solvent control-treated or PA-treated BAECs were trypsinized, washed, and pelleted into glass vials. Lipids were extracted as described previously,[13] dissolved in chloroform/methanol (2:1, v/v), and subjected to liquid chromatography–tandem mass spectrometry (LC-MS/MS) analysis. Total ceramide content was expressed as the sum of individual species, normalized to cell number. For aortic tissue, adventitial fat was removed from excised aortas, lipids were extracted, and tissue ceramide fractions were measured with the same technique, normalized to sample weight.

### Annexin V Apoptosis Assay

BAECs or HUVECs were treated with PA or with heat (70°C) and then were trypsinized, washed, resuspended in annexin V binding buffer (BD Biosciences), and stained with annexin V–fluorescein isothiocyanate. Flow cytometric analysis was performed using a FACSCalibur system (BD Biosciences); 5000 events were acquired and analyzed per experimental sample.

### Proliferation Assay

BAECs were seeded at 5000 cells per well for 24 hours in complete medium, serum-starved in 0.1% BSA–Dulbecco's modified Eagle's medium, pretreated with PA, and stimulated with 25 to 50 ng/mL VEGF. Cell proliferation was measured at 0, 24, and 48 hours after VEGF treatment using a CellTiter-Glo assay (Promega, Madison, WI) based on ATP content in quadruplicate wells.

### PP2A Phosphatase Activity Assay

PP2A activity was measured using a PP2A immunoprecipitation phosphatase assay kit (EMD Millipore) according to the manufacturer's recommendations. In brief, PP2A was immunoprecipitated from BAEC lysates with anti-PP2A C subunit antibody (clone 1D6). Phosphopeptide substrate (KRpTIRR) was added to washed immunoprecipitates in Ser/Thr assay buffer and incubated for 10 minutes at 30°C, after which the amount of phosphate released from the phosphopeptide was measured by absorbance at 650 nm using malachite green solution and phosphate standard. The amount of released phosphate was normalized to the amount of PP2A C subunit detected by immunoblotting. Specificity of the PP2A was confirmed by blocking PP2A activity with 100 nmol/L OkA added both to cells and to the lysis buffer.

### MicroSPECT–CT Imaging

MicroSPECT–CT hindlimb imaging, detecting a $^{99m}$Tc-labeled chelate-peptide conjugate containing an RGD (Arg-Gly-Asp) motif (GE Healthcare, Little Chalfont, UK) targeted at the activated $\alpha_v\beta_3$ integrin was performed on ischemic and contralateral nonischemic hindlimbs as described previously.[14] In brief, animals were injected intravenously with 1 mCi of the $^{99m}$Tc-labeled chelate–peptide conjugate containing an RGD

motif ($^{99m}$Tc-NC100692; GE Healthcare) targeted at the activated $\alpha_v\beta_3$ integrin at 4 days and 4 weeks after surgical induction of hindlimb ischemia. Our previous experiments have validated specific signals and counts from $^{99m}$Tc-NC100692, relative to a control scrambled peptide ($^{99m}$Tc-AH-111744-01) that yields minimal background counts in angiogenic tissues.[14] Imaging with the control peptide confirmed these prior results (data not shown).

Imaging was performed with a hybrid dual-head micro-SPECT—CT small-animal scanner (Gamma Medica X-SPECT; Siemens Healthcare, Malvern, PA) equipped with 1-mm pinhole collimators. Animals were placed on the animal bed in the supine position, with hindlimbs secured in an extended position. At 1 hour after radiotracer injection, mice underwent SPECT imaging (32 projections, 60 seconds/projection per scanner head) with a 20% energy window centered at 140 keV. This was followed by high-resolution anatomical CT imaging (512 projections at 50 kVp/600 μA energy).

MicroSPECT and CT images were reconstructed as described previously.[14] In brief, MicroSPECT images were filtered, fused with microCT images, and converted to Analyze 7.5 file format (Mayo Foundation, Rochester, MN). The relative tracer uptake within the hindlimb soft tissues was quantified using semiautomated software (BioImage Suite version 2.6; Yale University School of Medicine, New Haven, CT). Complex irregular volumes of interest (VOIs) were generated from the microCT images and were registered with the microSPECT images. These complex regions included only soft-tissue structures from the hindlimb; skeletal structures were removed during the segmentation process. The object map was applied to the corresponding microSPECT image to determine mean counts in each VOI. The radiotracer activity from the ischemic (I) proximal and distal hindlimb was normalized by the contralateral non-ischemic (NI) proximal and distal hindlimb, respectively, to compute I/NI ratios.

### Statistical Analysis

Student's *t*-test or repeated measures analysis of variance were used, as applicable. $P < 0.05$ was considered significant.

## Results

### PA Attenuates Basal and VEGF-Induced NO Production

To determine whether PA affects endothelial NO production, BAECs were pretreated for 3 hours with vehicle control or BSA-conjugated PA, before measurement of basal and 100 ng/mL VEGF-stimulated NO by chemiluminescence. We observed a 50% reduction in basal NO production in cells treated with 100 μmol/L PA, and an abrogation of the VEGF-induced augmentation in NO production (Figure 1A). These findings demonstrate that arterial ECs exposed *in vitro* to PA levels even below those observed in individuals with metabolic syndrome exhibit diminished basal and VEGF-stimulated NO production.

### PA Impairs VEGF-Induced Angiogenesis *in Vitro*

VEGF plays a significant role in angiogenic responses through its modulation of eNOS activity and NO production.[15] The Matrigel cord formation assay is an accepted *in vitro* model for study of critical endothelial features required for angiogenesis (ie, those of matrix plus growth factor-driven EC proliferation and migration). HUVECs were plated in growth factor—reduced Matrigel to assess the effects of PA on angiogenic cord formation. Cord length, area, and branch point (node) numbers were assessed after 12 hours in vehicle control or 100 μmol/L PA, with and without 100 ng/mL VEGF. We observed a marked reduction in visible VEGF-induced cord formation in the PA-treated wells (Figure 1C); quantification indicated approximately 50% reduction in all angiogenesis correlates (Figure 1D). At PA concentrations of ≥300 μmol/L, cord formation was absent (data not shown).

To ensure that the loss of BAEC NO production and HUVEC-based angiogenic cord formation was not a consequence of PA-induced apoptosis, PA-treated BAECs (100 and 300 μmol/L for 3 hours) and HUVECs (100 and 300 μmol/L for 16 hours) were analyzed by fluorescence-activated cell sorting for annexin V binding. The 3-hour and 16-hour time points were chosen to correlate with those used in BAEC signaling and HUVEC Matrigel assays, respectively. Annexin V positivity in PA-treated, non-permeabilized BAECs and HUVECs was negligible, compared with heat-induced apoptotic controls (Figure 1B). Thus, the relative NO deficiency states in PA-treated ECs was not a consequence of PA-induced EC apoptosis. However, PA significantly reduced BAEC proliferation in response to VEGF (Figure 1E), suggesting that PA may impair proangiogenic proliferative signaling downstream of VEGFR2.

### PA Inhibits VEGF-Induced Akt and eNOS Phosphorylation

VEGFR2, the dominant VEGF receptor in mature endothelium, is a major mediator of the mitogenic, angiogenic, and permeability-enhancing effects of VEGF. The most proximal step in the VEGF signaling cascade is ligand-induced VEGFR2 dimerization and trans-autophosphorylation. To assess whether PA-induced defects in VEGF-stimulated NO production are a consequence of impaired VEGFR2 activation, BAECs were treated with 0 (vehicle control) or 100 μmol/L PA. At 3 hours, cells were stimulated with 50 ng/mL VEGF for 10 minutes, after which lysates were recovered for VEGFR2 immunoprecipitation and phosphotyrosine immunoblotting. VEGF-stimulated VEGFR2 tyrosine phosphorylation was not impaired by 100 μmol/L PA (Figure 2A),

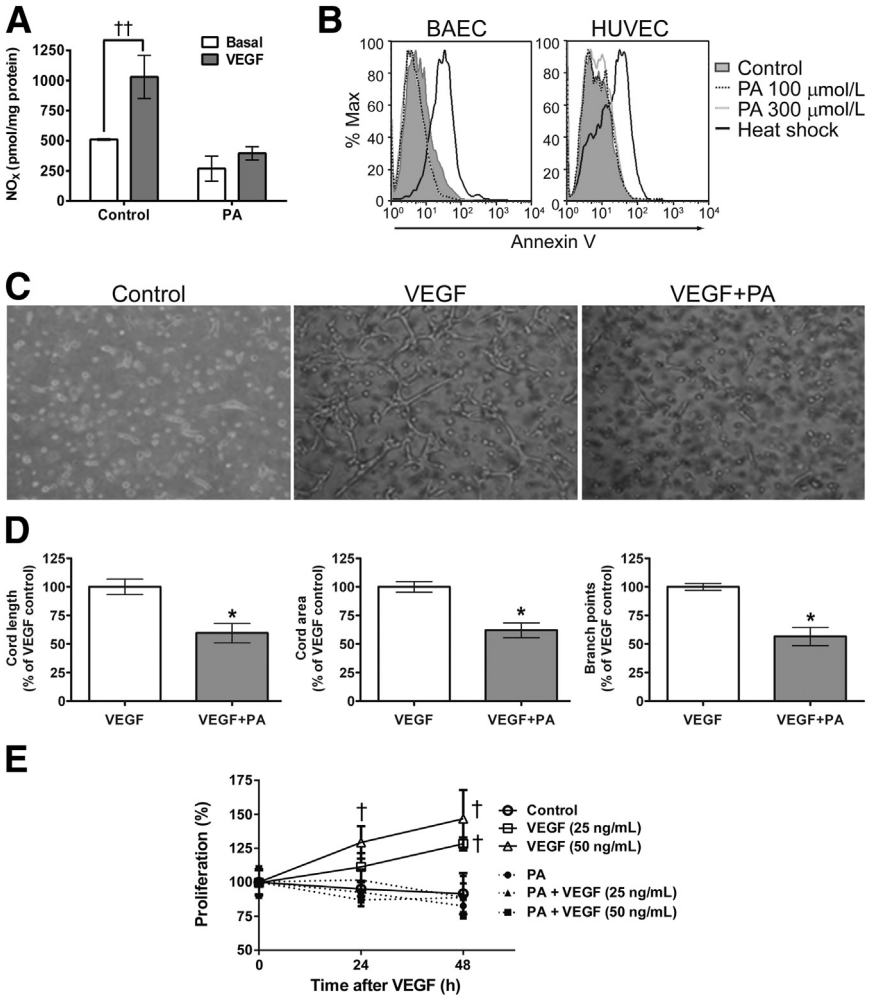


**Figure 1** Effect of PA on VEGF-induced EC NO release and angiogenic cord formation. **A:** Basal and VEGF-induced NO release in BAECs. BAECs were treated with 100 μmol/L PA or solvent control for 4 hours, followed by 100 ng/mL VEGF or control for 45 minutes, after which $NO_x$ was measured by chemiluminescence. **B:** PA does not induce EC apoptosis. BAECs or HUVECs were treated with vehicle control or PA at 100 or 300 μmol/L for 3 and 16 hours, respectively. For positive apoptotic controls, cells were heat shocked at 70°C for 5 minutes before annexin V staining. **C:** PA effect on Matrigel cord formation. HUVECs were treated with 100 μmol/L PA and 100 ng/mL VEGF. **D:** Metamorph analysis was used to quantify cord length, area, and branch points in representative fields. **E:** PA pretreatment impairs VEGF-induced proliferation. BAECs were seeded in 96-well plates, serum starved, and pretreated with 100 μmol/L PA before stimulation with VEGF. Cell proliferation was measured using a CellTiter-Glo assay in quadruplicate wells. Data are expressed as means ± SEM (**A** and **D**) or as means ± SD (**E**) and are representative of three independent experiments. $^{*}P <$ 0.05 versus VEGF alone; $^{\dagger}P < 0.05$, $^{\dagger\dagger}P < 0.005$ versus control. Original magnification, ×400.

despite the profound effect of this PA treatment on stimulated NO production (Figure 1A). There was no PA effect on total VEGFR2 levels. Higher PA concentrations did have an inhibitory effect on VEGFR2 phosphorylation (data not shown). However, because all of the PA-induced defects (ie, NO production and angiogenic cord formation, as well as distal kinase signaling, which is discussed below) could be reproducibly detected in the presence of 100 μmol/L PA, we focused on those more distal consequences of PA on the VEGF signaling cascade. For further experiments, PA treatments were at 50 or 100 μmol/L.

VEGFR2-$Tyr^{1175}$ is an autophosphorylation docking site that initiates PLC-γ—ERK1/2 and PI3K—Akt pathway activation. Akt—eNOS and ERK activation are all critical in a variety of growth factor—stimulated angiogenic responses at the cellular and tissue level, including cell migration, proliferation, antiapoptosis, and tissue remodeling. We therefore assessed the effect of PA on VEGF-stimulated phosphorylation on the following critical kinase activation sites: Akt-$Ser^{473}$, eNOS-$Ser^{1179}$, and ERK1-$Thr^{202}$/ERK2-$Tyr^{204}$. As before, BAECs were treated with 0 (vehicle control) or 100 μmol/L PA for 3 hours, followed by 10 minutes of 0 (control) or 50 ng/mL VEGF treatment, after which lysates were recovered for immunoblotting. We observed a dose response from 10 to 100 μmol/L for this PA-induced inhibition (Figure 2B). PA at 100 μmol/L, a concentration that does not affect VEGF-stimulated receptor phosphorylation, imparted a strong inhibition of VEGF-induced Akt, eNOS, and ERK activation (Figure 2, C—E). These results indicate that activation, as determined by activation site phosphorylation in multiple key kinases downstream of VEGFR2 signaling, is impaired in PA-exposed ECs.

## FFA-Induced eNOS Activation Defect Is Not VEGF-Specific

Because the PA-induced inhibitory effect on VEGF-stimulated NO production is largely the result of ceramide-activated, PP2A-mediated (discussed below) Akt and eNOS dephosphorylation, we expected that similar biochemical changes would be observed in the context of other eNOS agonists. Bradykinin-stimulated eNOS phosphorylation was greatly reduced in PA-exposed cells (Figure 2F). The diversity of signaling defects, both to receptor tyrosine kinase and G protein-coupled receptor

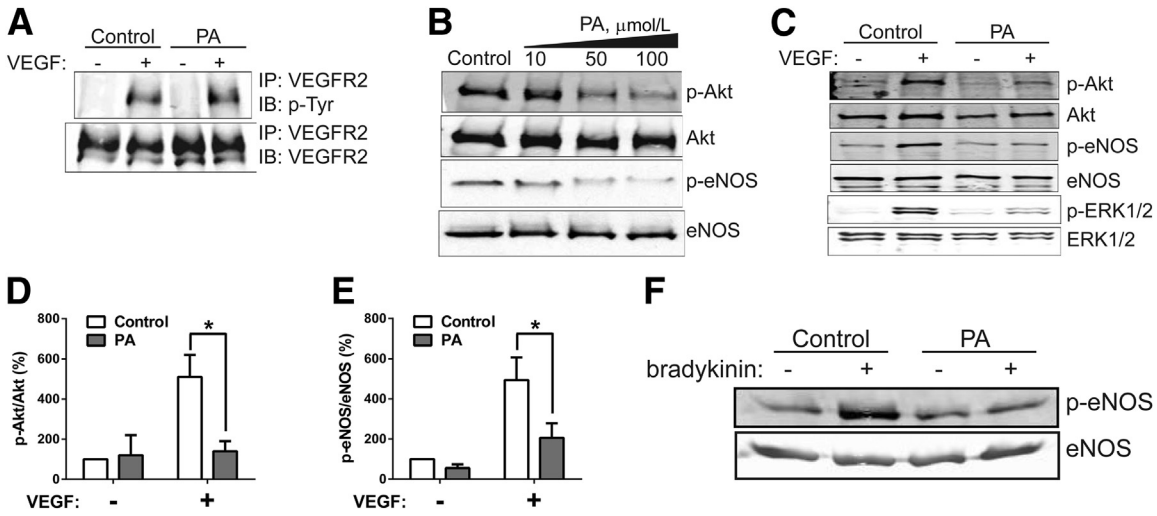


**Figure 2** **A:** Effect of PA on stimulus-dependent kinase activation. BAECs were pretreated for 3 hours with vehicle control or 100 μmol/L PA, followed by 0 or 100 ng/mL VEGF treatment for 10 minutes. Effect of PA on VEGF-induced VEGFR2 tyrosine phosphorylation, by VEGFR2 immunoprecipitation and phosphotyrosine immunoblotting. **B:** Dose response of VEGF-induced Akt and eNOS phosphorylation after pretreatment with 0, 10, 50, or 100 μmol/L PA. All samples were then treated with 100 ng/mL VEGF for 10 minutes. **C:** Representative immunoblot showing effects of PA on phosphorylation of Akt, eNOS, and ERK1/2. **D:** Densitometry of Akt phosphorylation at $Ser^{473}$. **E:** Densitometry of eNOS phosphorylation at $Ser^{1179}$. **F:** Effect of PA on bradykinin-induced phosphorylation of eNOS at $Ser^{1179}$. Data are expressed as means ± SEM. $n = 3$ (**D**); $n = 5$ (**E**). *$P < 0.05$. IB, immunoblotting; IP, immunoprecipitation.

agonists, supports a state of extensive endothelial dysfunction induced by PA.

## PP2A Mediates PA-Induced Impairment in VEGF-Stimulated Angiogenic Kinase Activation

As with most molecules that are dynamically regulated by phosphorylation, the aforementioned kinase activation states are a net consequence of phosphorylation and dephosphorylation. Because the Akt—eNOS and ERK pathways diverge proximally, we investigated whether the relative lack of activation of all three kinases is a consequence of PA-induced enhanced dephosphorylation. Akt, eNOS, and ERK 1/2 are all substrates of PP2A, an abundant protein known to regulate these kinases[16–18] by colocalizing in specific cellular compartments. That is, augmented PP2A interaction results in kinase inactivation. We therefore performed a series of coimmunoprecipitation experiments. PA exposure dramatically enhanced PP2A association with eNOS, ERK and Akt (Figure 3A and Supplemental Figure S1). These findings are consistent with PA impairing endothelial responses to VEGF through promoting PP2A interactions with critical enzymatic substrates, thereby reducing NO production. In addition, we performed PP2A phosphatase activity assays, using a fluorimetric phosphopeptide substrate (KRpTIRR). Both PA and ceramide (discussed below) induced a sustained, significant increase in EC PP2A enzymatic activity (data not shown).

To further verify the role of PP2A in relevant kinase regulation, we tested whether the phosphatase inhibitor OkA, a specific PP2A inhibitor at the dose of 100 nmol/L, prevents the aforementioned defects observed in PA-exposed, VEGF-treated BAECs. The BAECs were pretreated with OkA for 30 minutes before 3-hour exposure to 100 μmol/L PA, after which cells were treated with 0 or 50 ng/mL VEGF for up to 20 minutes. OkA prevented the reduction in VEGF-stimulated eNOS-$Ser^{1179}$ phosphorylation observed in PA-exposed cells (Figure 3B). Similar results were obtained when assessing Akt-$Ser^{473}$ phosphorylation (data not shown). These rescue experiments support the notion that the PA-induced defects in VEGF signaling occur through activation of endothelial PP2A.

## PA Generates Endothelial Ceramides

Saturated fat elevates ceramide levels in liver and muscle, with some fat-induced insulin signaling abnormalities prevented by ceramide synthesis inhibition.[19] Furthermore, PP2A is one of the ceramide-activated protein phosphatases.[20] We therefore investigated whether PA-induced ceramide generation is a central component of the endothelial signaling defects described above. Individual ceramide species in control and PA-treated BAECs were measured by LC-MS/MS; total ceramide content was expressed as the sum of individual species and normalized to cell number. We observed a twofold and sixfold ceramide increase in BAECs exposed to PA for 3 and 18 hours, respectively (Figure 4, A and B). Most of the ceramide elevation is in the early species C16, suggesting generation via the *de novo* pathway, in which C16 is generated by a series of enzymatic reactions on palmitoyl CoA (C16:O) binding to serine. The augmented endothelial ceramide levels are greater than those reported to cause significant cellular and pathological abnormalities.[21]

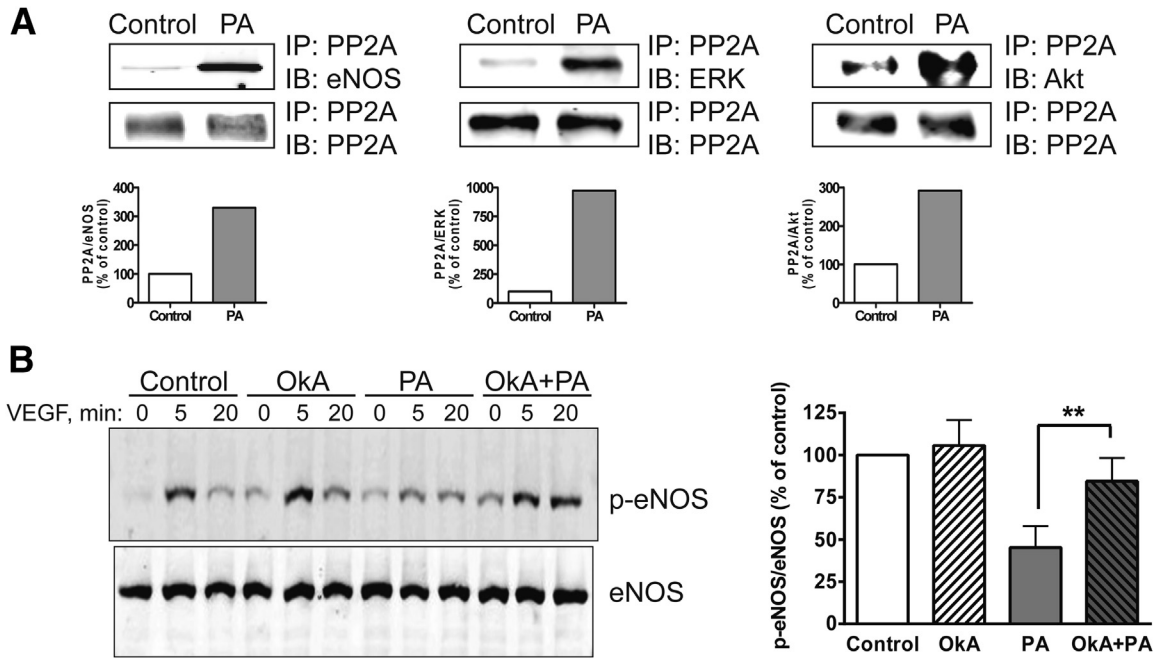


**Figure 3** Role of PP2A in PA-induced VEGF signaling defect. **A:** Coimmunoprecipitation of PP2A and eNOS, ERK, and Akt in BAECs. For densitometric quantification, the control ratio was defined as 100%. The reverse coimmunoprecipitations are presented in Supplemental Figure S1. **B:** Effect of PP2A inhibition on VEGF-induced eNOS-Ser$^{1179}$ phosphorylation. BAECs were pretreated for 4 hours with 100 μmol/L PA or control in the presence or absence of 100 nmol/L PP2A inhibitor OkA. Cells were then treated with 100 ng/mL VEGF for 0, 5, or 20 minutes. For densitometric quantification of p-eNOS/total eNOS in VEGF 5-minute samples, the control ratio was defined as 100%. Data are expressed as means ± SEM. Blots and data are representative of three independent experiments. $^{**}P < 0.01$.

## PA-Induced Endothelial Ceramide Generation Causes Defects in VEGF Signaling and VEGF-Induced Angiogenic Cord Formation

In determining whether the ceramide generation in PA-exposed cells is responsible for the aforementioned endothelial defects, we first attempted to reproduce those defects by raising intracellular ceramide levels with the short-chain, cell-permeable C2 ceramide. The C2 ceramide treatment resulted in abrogation of VEGF-induced eNOS-Ser$^{1179}$ and Akt-Ser$^{473}$ phosphorylation, as well as in reduction of basal levels of p-eNOS and p-Akt (Figure 4C). The expected reduction in VEGF-stimulated NO production was also detected (Figure 4D), similar to that observed in the presence of PA (Figure 1A). Furthermore, C2 ceramide treatment of HUVECs prevented all aspects of VEGF-induced cord formation (area, length, and branch points) in the Matrigel *in vitro* assay (Figure 4, E and F), similar to the PA effect. Thus, the endothelial defects in VEGF responses induced by PA can all be reproduced by raising intracellular ceramide levels with C2 ceramide.

In our model, PA exposure leads to the endothelial accumulation of excess palmitoyl CoA moieties, with consequent *de novo* ceramide synthesis. The rate-limiting step in this biosynthetic pathway is catalyzed by serine palmitoyl transferase (SPT), generating ketosphinganine from palmitoyl CoA and serine. Myriocin is a potent and specific SPT inhibitor[22] that binds to both the LCB1 and LCB2 subunits.[23] To investigate whether inhibiting *de novo* ceramide synthesis protects ECs from PA-induced VEGF signaling defects, BAECs were pretreated with 100 nmol/L myriocin for 30 minutes before the 3-hour exposure to PA, followed by VEGF stimulation and kinase activation analysis. Myriocin partially prevented the PA-induced inhibition of VEGF-stimulated eNOS phosphorylation (Figure 5A). Again, as expected given these signaling results, myriocin partially rescued VEGF-stimulated angiogenic cord formation by PA-treated HUVECs in the Matrigel *in vitro* assay (Figure 5B). We observed approximately 50% reduction of the PA-induced inhibition of all three aspects of cord formation (Figure 5C). Myriocin largely (but incompletely) prevented PA-induced increases in C16 and total ceramide generation (Supplemental Figure S2) ($P < 0.007$ versus control or PA), which explains the significant but incomplete rescue of VEGF-stimulated responses.

## High-Fat Feeding Impairs Responses to VEGF *in Vivo*

To investigate the effects of saturated fatty acids on VEGF responses *in vivo*, AKR/J mice were fed a high-fat diet, such that 60% of the caloric intake was derived from saturated fats (and predominantly from PA). Dietary fat composition determines the pattern of FFA elevation.[24] After 2.5 weeks of high-fat feeding, there was a 71% increase in FFA levels, relative to control-chow feeding (Figure 6A). Similar FFA

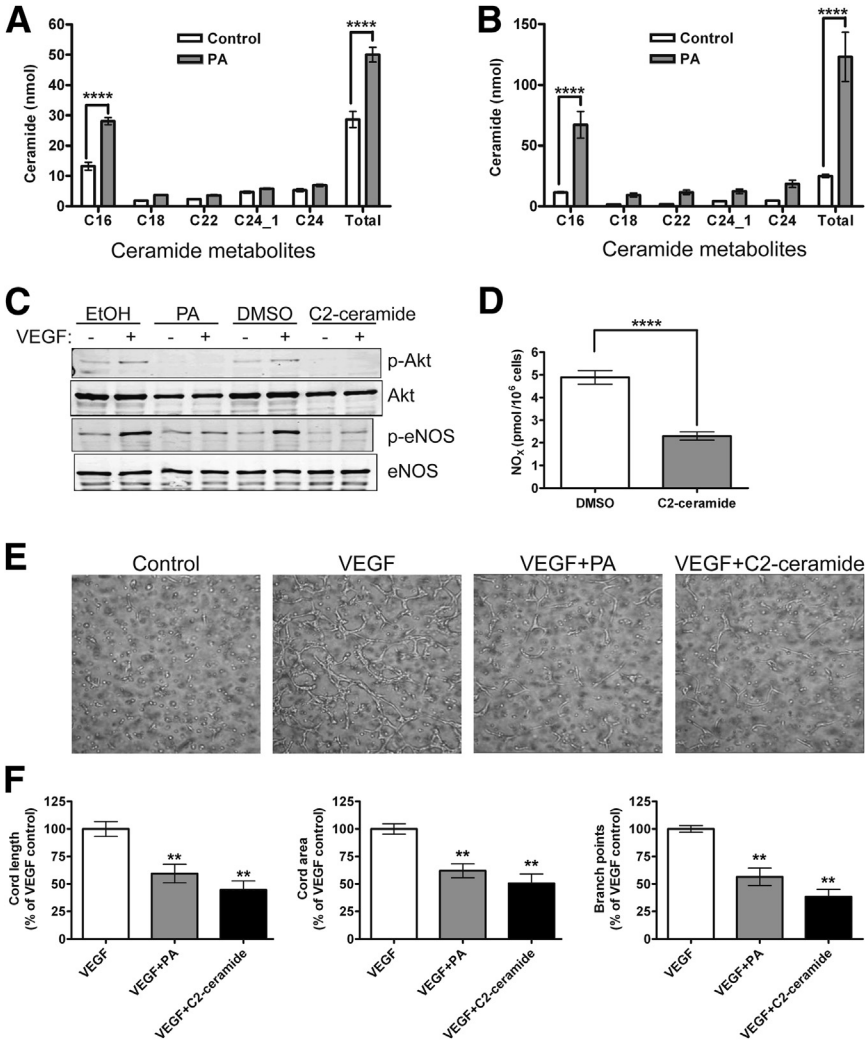


**Figure 4** Comparison of ceramide-induced and PA-induced effects on VEGF-stimulated NO production and angiogenic cord formation. **A** and **B:** BAECs were treated with 100 μmol/L PA for 4 hours (**A**) or 18 hours (**B**), after which cells were recovered, lipids were dissolved in methanol, and ceramide fractions were measured by LC-MS/MS. Total ceramide content (ie, the sum of the individual species) was normalized to cell number. **C** and **D:** Directly raising intracellular ceramide with 30 μmol/L C2 ceramide mimics defects caused by exposure to 100 μmol/L PA in 100 ng/mL VEGF-induced p-Akt-Ser$^{473}$ and p-eNOS-Ser$^{1179}$ (**C**) and NO production measured by chemiluminescent $NO_x$ analysis (**D**). Blots are representative of three independent experiments. **E:** Similar effects were seen in Matrigel cord formation. Images for VEGF plus ethanol solvent control or dimethyl sulfoxide control were identical to the VEGF image (data not shown). **F:** Cord length, area, and branch points were quantified with Metamorph analysis. Images and quantification are representative of three independent experiments. Data are expressed as means ± SEM. $^{**}P < 0.01$, $^{****}P < 0.0001$ versus control or VEGF. Original magnification, ×400.

elevations were observed in high-fat-fed C57BL/6J mice (discussed below). There was a minimal and statistically nonsignificant increase in weight of the high-fat-fed animals (data not shown). Most models of dietary insulin resistance involve substantially longer periods of high-fat feeding. Our goal in the present study was to develop a model with elevated serum FFA levels without significant insulin resistance, and so the duration of fat-feeding was abbreviated.

To recapitulate the *in vitro* VEGF signaling defect *in vivo*, 1 mg recombinant VEGF-$A_{165}$ was infused intravenously into mice fed a high-fat or a control diet. After 10 minutes, the animals were perfused with 1 mmol/L $Na_3VO_4$ for 3 minutes; aortas were then harvested and homogenized, after which p-eNOS and p-Akt immunoblotting was performed. The loss of VEGF induced aortic eNOS-Ser$^{1177}$ phosphorylation in high-fat-fed animals (Figure 6B). Although less profoundly and less consistently reduced than p-eNOS, Akt-Ser$^{473}$ phosphorylation was less robust in aortas obtained from mice fed a high-fat diet. Because the aortic homogenates contain a combination of cells and because Akt is ubiquitously expressed, whereas eNOS is endothelial specific within the aorta (and therefore is VEGF responsive), more impressive effects of high-fat feeding on eNOS phosphorylation were expected. The fat-induced inhibition of VEGF-stimulated eNOS activation was similar to that observed with PA-exposed ECs *in vitro*.

To extend these aortic signaling experiments to VEGF-induced angiogenesis *in vivo*, $1 \times 10^8$ viral particles of recombinant adenovirus encoding VEGF (AdVEGF) or Cre recombinase control (AdCre) were injected intradermally into the left and right ears, respectively, of AKR/J mice. Ears were harvested at 5 days, at which point VEGF-induced angiogenic responses and capillary leak occur. A robust VEGF response was observed in mice fed the control diet (Figure 6C). The thickness and length of the neovessels, as well as the erythema (capillary leak), were attenuated in the ear of mice fed a high-fat diet (Figure 6C). This observation was confirmed by CD31/PECAM immunofluorescent staining, with far fewer, thinner and shorter CD31/PECAM-positive (capillary) structures in the ear of mice fed a high-fat diet (Figure 6D). This difference was quantified by image analysis, which confirmed a 45% reduction in

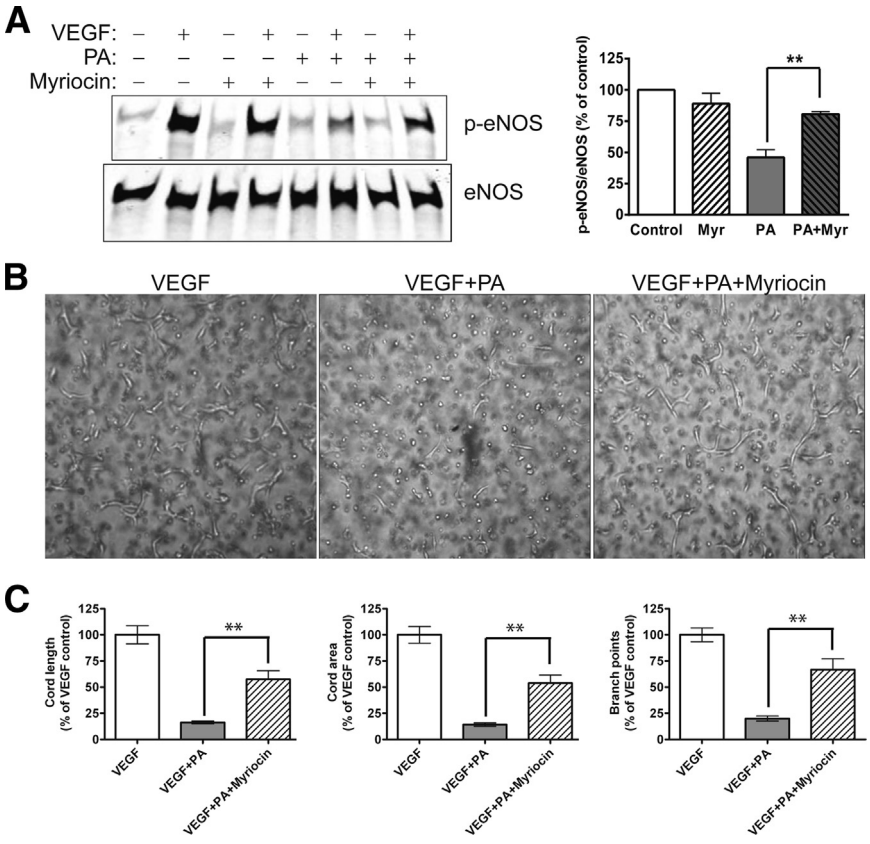


**Figure 5** Effect of ceramide synthesis inhibition on PA-induced VEGF signaling defects. **A:** Effect of treatment with 100 nmol/L myriocin, a serine palmitoyltransferase (ceramide synthesis) inhibitor, on VEGF-induced p-eNOS $Ser^{1179}$ in BAECs exposed to 100 μmol/L PA or control for 4 hours. **B:** Effect of myriocin on 100 ng/mL VEGF-induced Matrigel cord formation in HUVECs in the presence or absence of 100 μmol/L PA ± 100 nmol/L myriocin. **C:** Cord length, area, and branch points were quantified with Metamorph analysis. Blots, images, and quantification are representative of three independent experiments. $^{**}P < 0.01$. Original magnification, ×400. Myr, myriocin.

VEGF-induced capillary formation in the ear of mice fed a high-fat diet, compared with the controls (Figure 6E). In this model, AdVEGF is a potent stimulus to angiogenesis, with extensive capillary leak and capillary network formation. Although significant, the reduction in angiogenesis observed in mice fed a high-fat diet likely underestimates the effect of FFA on VEGF-induced endothelial responses, including angiogenesis in more physiological settings.

## High-Fat Feeding Increases Aortic Ceramide and Impairs Ischemia-Induced Arteriogenesis

Because the *in vitro* findings demonstrated that PA-induced ceramide generation is mechanistically linked to the signaling defects noted, we measured ceramide levels in aortic tissue recovered from mice fed a high-fat or control diet for 2.5 weeks. We observed an elevation in early ceramide species (C16, C18, and C22) in aortas from mice fed a high-fat diet, relative to control mice (Figure 7A). These differences, although modest, were statistically significant and, we believe, biologically important. The pattern of ceramide elevation is consistent with *de novo* generation from excessive palmitoyl CoA, similar to that observed for EC ceramide generation *in vitro*.

Ischemia-driven neovessel formation involves endothelial responses to multiple angiogenic growth factors, including VEGF. Murine hindlimb ischemia is an established model of ischemia-driven angiogenesis and arteriogenesis. Of the several different technical approaches, we chose the most severely ischemic and hypoxic model, which provides a potent stimulus to VEGF-induced neovessel formation. The femoral artery and vein of 2.5 weeks high-fat-fed and control C57BL/6J mice were ligated just below the inguinal ligament and at the level of the popliteal artery, after which this entire vascular segment was removed. Hindlimb perfusion was serially measured on postoperative days 3, 7, and 21, using a laser Doppler vascular probe, placed directly on the gastrocnemius muscle, both in the ischemic and the contralateral normal hindlimb. Data are expressed as ischemic/normal flow ratios. Angiogenic recovery was slower in the mice fed a high-fat diet, compared with controls, and the most dramatic differences were observed at the earlier postoperative time points (Figure 7B). This is consistent with previous reports that, in animal models of severe limb ischemia, VEGF levels rise rapidly after ischemia induction and taper quickly.[25,26] The flows at early time points (3 and 7 days) are most reflective of angiogenic responses, whereas contributions of collateral arteriogenesis occur at later time points.

To obtain a more precise analysis of ischemia-induced arteriogenesis at later time points, we also performed *in vivo* hybrid SPECT–CT imaging, using the $^{99m}$Tc-labeled RGD (Arg-Gly-Asp) peptide NC100692 (GE Healthcare), which specifically binds activated $\alpha_v\beta_3$ integrin with high affinity.[27] This cyclic peptide has been used to target peripheral neovascularization in response to ischemia in models similar to those described

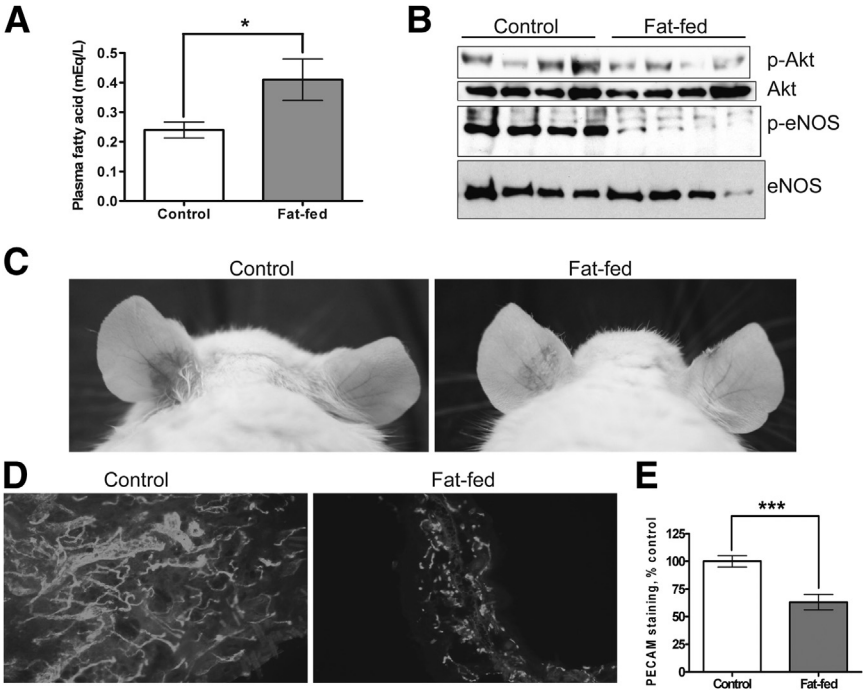


**Figure 6** Effect of high-fat feeding (saturated fatty acid) on VEGF-induced angiogenic kinase phosphorylation and angiogenesis *in vivo*. **A:** AKR/J mice were fed a high-fat diet (60% saturated fat—based calories) or a normal chow diet for 3 weeks. Plasma nonesterifed FFAs were measured by an acyl-CoA oxidase-based colorimetric assay. **B:** VEGF-$A_{165}$ (1 mg) was infused intravenously for 10 minutes, after which aortas were harvested and homogenized, and tissue lysates were immunoblotted for p-Akt-$Ser^{473}$, p-eNOS-$Ser^{1177}$, total Akt, and total eNOS. Each lane represents an individual mouse, and blots are representative of three independent experiments. **C:** AdVEGF (left ear) or AdCre (right ear) were injected intradermally into high-fat-fed or control mice. Ears were photographed at 5 days for vascularity and vascular leak. **D** and **E:** Ears were fixed and immunostained for CD31/PECAM expression (**D**), and data were quantified with ImageJ analysis, normalizing AdVEGF (left ear) pixels with the corresponding AdCre (right ear) pixels (**E**). The control ratio was defined as 100%. Data are expressed as means ± SEM. $*P < 0.05$, $***P < 0.001$. Original magnification, ×400.

here.[14,28] The semiautomated quantitative approach, with CT-generated VOIs in which relative radiotracer activity is serially determined by micro-SPECT imaging, has been validated previously.[14] Both $\alpha_v\beta_3$ expression and activity levels are increased in angiogenic settings, where this integrin plays a role in cell migration, proliferation, and survival[29] and can be VEGFR2-associated.[30]

In our severe ischemia model, serial hindlimb imaging was performed on the same animals over a 4-week postoperative period. Representative microSPECT—CT images show the CT-generated VOIs and the $\alpha_v\beta_3$—specific radioligand uptake in those VOIs, at 4 days and 4 weeks after femoral artery ligation in high-fat-fed and control mice (Figure 7C). Quantification was expressed as the ratio of ligand uptake in the ischemic to the contralateral nonischemic hindlimb in the proximal hindlimb (Figure 7D). Imaging at early time points is difficult to interpret with this ligand, because the inflammation induced both by surgery and by ischemia promotes recruitment of leukocytes (largely monocytes and macrophages) expressing $\alpha_v\beta_3$. As expected, ligand uptake was high, and differences between control and mice fed a high-fat diet were obscured at 4 days. However, proximal hindlimb imaging at 4 weeks demonstrated a significant reduction in activated $\alpha_v\beta_3$ expression in the mice fed a high-fat diet. This later time point is most reflective of differences in collateral arteriogenesis, and is more easily seen proximally. There was also a nonsignificant trend toward less uptake at later time points in the distal hindlimb, but this was less dramatic (data not shown). The two techniques, laser Doppler imaging over the distal hindlimb at early time points, and proximal $\alpha_v\beta_3$ SPECT imaging at later time points, thus reflect impaired microvessel angiogenic and collateral arteriogenic responses, respectively, in short-term high-fat-fed animals. Both adaptive responses to ischemia are impaired, and the two techniques are complementary.

## Aortic Ceramides Are Reduced and VEGF Responses Are Restored in High Fat—Fed SPT Haploinsufficient Mice

Because the PA-induced alterations in VEGF-induced Akt and eNOS phosphorylation are ceramide-mediated *in vitro*, we used a genetic model to address the importance of ceramide generation *in vivo*. The $Sptlc2^{-/+}$ mouse is haploinsufficient in endogenous ceramide synthesis.[8] For confirmation in vascular tissue, $Sptlc2^{-/+}$ mice were fed a high-fat diet, as above, for 2.5 weeks, after which aortas were harvested for individual ceramide species measurement by LC-MS/MS. Aortic ceramide levels in $Sptlc2^{+/+}$ and $Sptlc2^{-/+}$ mice fed normal chow were essentially identical (Figure 8A). However, the increase in ceramide metabolites observed in high-fat-fed $Sptlc2^{+/+}$ mice was largely (>60%) prevented in $Sptlc2^{-/+}$ mice (Figure 8B). This relative impairment in fat-induced ceramide synthesis provided an opportunity to correlate the VEGF resistance mechanism (ceramide-driven) that we established *in vitro* with the *in vivo* impairment described above. $Sptlc2^{-/+}$ mice were relatively protected from the fat-induced inhibition of VEGF signaling, as observed in aortic tissue p-Akt and p-eNOS immunoblots after VEGF IV infusion (Figure 8, C—E) and in ear angiogenesis analysis after AdVEGF injection (Figure 8, F and G). These observations demonstrate that ceramide generation is fundamental to the VEGF resistance state induced by high-fat feeding *in vivo*.

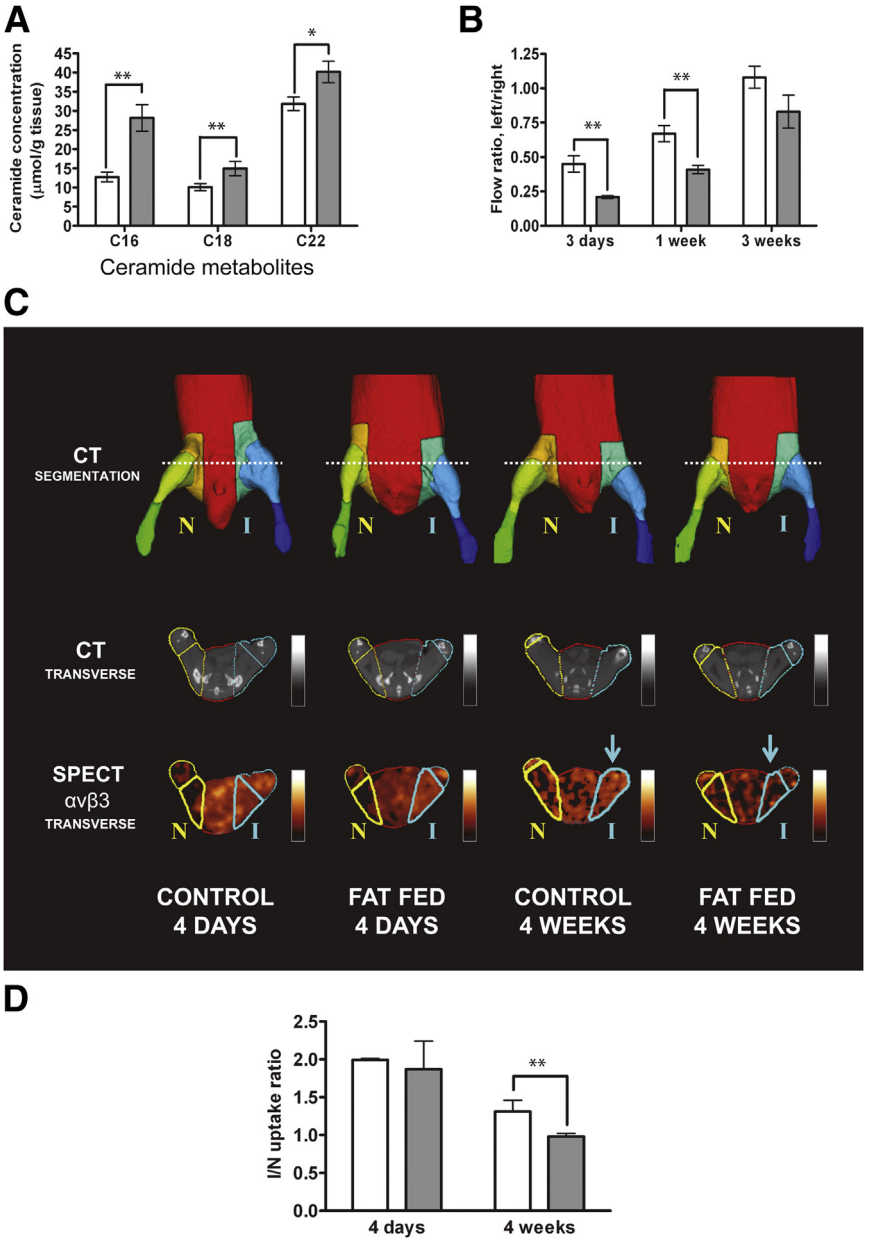


**Figure 7** Effect of high-fat feeding on vascular flow recovery to hindlimb ischemia. **A:** Aortas were recovered from C57BL/6J mice after 2 weeks of normal chow (white bars) or a high-fat (gray bars) diet. Adventitial fat was carefully excised, and tissue homogenates were analyzed for ceramide content by LC-MS/MS. **B:** C57BL/6J mice were fed normal chow or a high-fat diet for 2.5 weeks, after which unilateral (left) femoral artery ligation was performed. Laser Doppler imaging was performed at 3 days, 1 week, and 3 weeks after femoral artery ligation over the gastrocnemius muscle in C57BL/6J mice fed normal chow or a high-fat diet for 2.5 weeks. Left/right flow ratios refer to ischemic/nonischemic hindlimb. **C:** Arteriogenic response to hindlimb ischemia measured by microSPECT—CT in C57BL/6J mice fed normal chow or a high-fat diet at 4 days and 4 weeks after ligation. Representative images show the ischemic (I) left hindlimb and the control nonischemic (N) right hindlimb; a $^{99m}$Tc-labeled radiotracer was targeted at activated $\alpha_v\beta_3$. The microCT images were segmented to generate multiple VOIs (**top row**). Contours of these VOIs are superimposed on representative microCT images (**middle row**). These complex VOIs were applied to registered microSPECT images (**bottom row**), to determine mean counts in the proximal hindlimb VOI (**bold outline**). The quantification of activated $\alpha_v\beta_3$ is reflected in the colorimetric intensity scale (**bottom row**). **D:** Quantitative mean counts in ischemic proximal hindlimb VOI were normalized to the corresponding contralateral nonischemic hindlimb VOI and expressed as the I/N uptake ratio. **Arrows** point to the VOI in the ischemic hindlimb where the difference in the activated $\alpha_v\beta_3$ is apparent between control and fat-fed mice at 4 weeks after ligation. Data are expressed as means ± SD (**A**) or means ± SEM (**B** and **D**) and are representative of three independent experiments. $n = 10$ mice per group (**A** and **B**); and $n = 5$ per group (**D**). $^*P < 0.05$, $^{**}P < 0.01$.

## Discussion

Increased plasma FFA is one of the hallmarks of insulin resistance. Endothelial function, largely defined as endothelium-dependent vasodilation, is impaired in metabolic syndrome. Endothelial dysfunction has a strong and independent predictive value for atherosclerosis and for cardiovascular events.[2] A primary, causative role for FFA in cardiovascular disease has been suggested by experimental studies in which endothelial dysfunction has been induced by raising FFA levels in healthy individuals.[31] Paradoxically, systemic VEGF levels are elevated in atherosclerosis and in type 2 diabetes,[6] states in which endothelium-dependent vasodilation is impaired. Thus, it is reasonable to hypothesize that there exists a state of VEGF resistance, at the level of the endothelium, analogous to (but not necessarily mechanistically identical to) insulin resistance states. In the present study, we examined the effect of PA, one of the fatty acids most commonly found in the western diet, on endothelial responses to VEGF *in vitro* and *in vivo*. ECs exposed to PA, even at levels below those commonly observed in metabolic syndrome, have markedly diminished levels of VEGF-induced eNOS, Akt, and ERK phosphorylation at critical activation sites, despite preserved VEGF-stimulated VEGFR2 tyrosine phosphorylation.

Reduced eNOS (and Akt) phosphorylation in response to VEGF would be expected to result in less EC NO production, as we observed (Figure 1). It is possible that

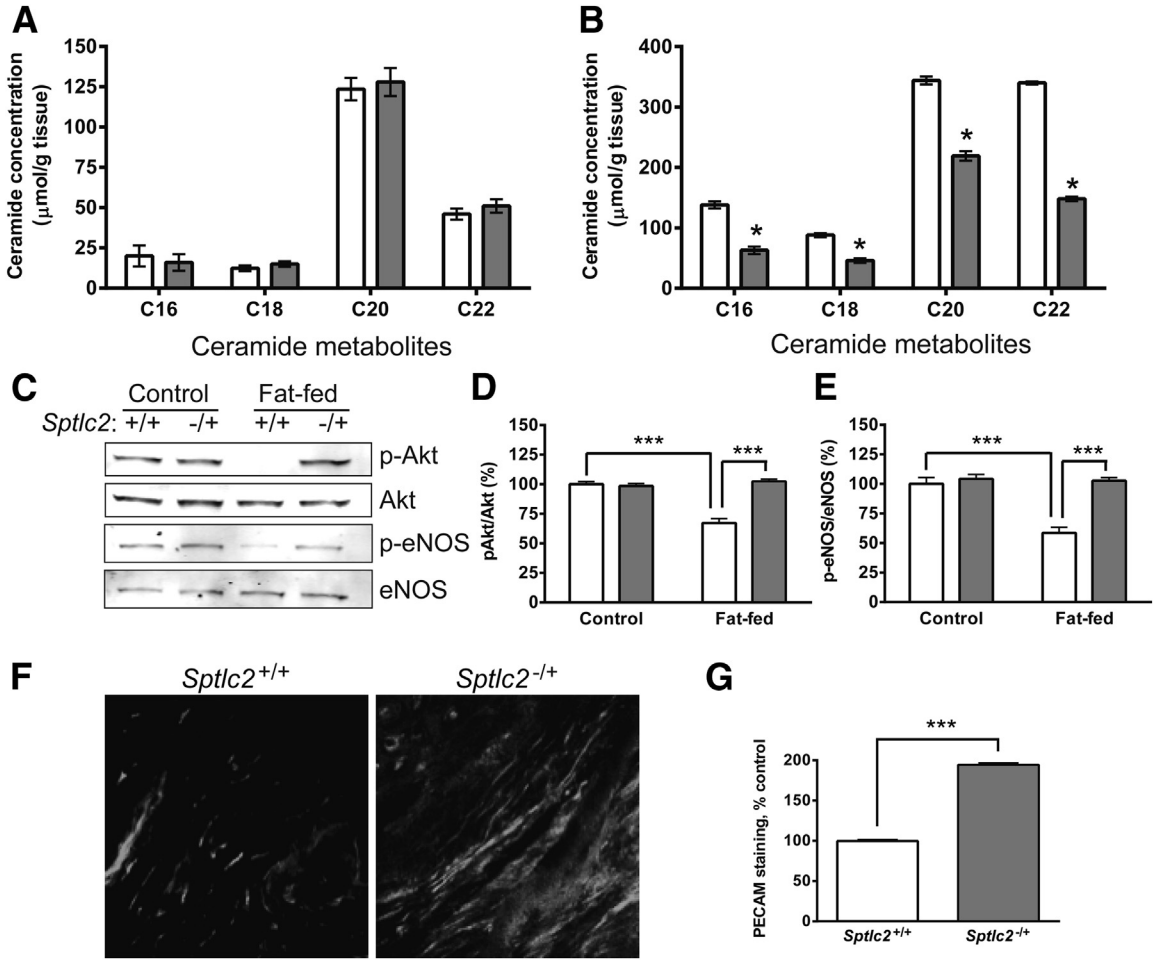


**Figure 8** Effect of SPT haploinsufficiency on aortic ceramide levels and angiogenic responses. **A** and **B:** Accumulation of ceramide metabolites in aortas of *Sptlc2*$^{-/+}$ (white bars) and *Sptlc2*$^{+/+}$ (gray bars) mice fed normal chow (**A**) or a high-fat diet (**B**) was analyzed by LC-MS/MS. **C**—**E:** VEGF-induced activation of Akt and eNOS in aortas of *Sptlc2*$^{-/+}$ and *Sptlc2*$^{+/+}$ mice fed normal chow or a high-fat diet was analyzed by immunoblotting. Representative immunoblots (**C**) and densitometry analyses (**D** and **E**). **F** and **G:** AdVEGF-induced angiogenesis in the ears of high-fat-fed *Sptlc2*$^{-/+}$ and *Sptlc2*$^{+/+}$ mice. Representative images (**F**) and quantitative analyses (**G**) are shown. Data are expressed as means ± SD (**A** and **B**) or as means ± SEM (**C**—**E** and **G**). $n = 3$ mice per group. $^{*}P < 0.05$, $^{***}P < 0.001$. Original magnification, ×400.

bioavailable NO is also diminished because of the production of reactive oxygen species (ROS), given that FFA-induced ROS generation has been demonstrated.[32] At the PA concentrations we used, there was no significant increase in EC ROS. Thus, although we believe that PA-induced increases in endothelial ROS generation could contribute to the endothelial dysfunction observed in metabolic syndrome, we were able to segregate and to study only those components of VEGF signaling abnormalities that are not ROS-dependent.

In addition to abnormal endothelial function, angiogenic and arteriogenic responses to ischemia are impaired in metabolic syndrome and diabetes.[33] The Matrigel angiogenic cord formation assay incorporates multiple aspects of VEGF-induced endothelial signaling required for angiogenic responses *in vivo*. These include Akt-dependent eNOS activation and NO release, as well as antiapoptosis and ERK-mediated cell-cycle transition. VEGF-treated, PA-exposed ECs are highly defective in their ability to form cords in Matrigel, consistent with an FFA-induced angiogenic defect.

Extending our study to *in vivo* analyses, we found that 2.5-week high-fat feeding led to significant elevations in plasma FFA and resulted in a marked impairment in VEGF-induced aortic eNOS and Akt phosphorylation. In addition, we used two *in vivo* models of VEGF-induced angiogenesis. Injected replication-deficient adenovirus encoding murine VEGF-$A_{164}$ into the ear of white mice provides an *in vivo* assay with which to assess a purely VEGF-driven angiogenic (and permeability) response. The dramatic decrease in VEGF-induced capillary neosynthesis in the mice fed a high-fat diet is consistent with the observed *in vitro* and *in vivo* VEGF signaling defects. We note, however, that the 2.5-week duration of high-fat feeding in the present study is much shorter than the 12 to 14 weeks common in metabolic studies in which marked weight gain and frank diabetes occur.[34]

Our second *in vivo* angiogenesis model was one of severe ischemia and hypoxia, in which VEGF-dependent responses

are critical in early phases of tissue recovery.[26] Postischemic microvessel angiogenic responses were significantly impaired in mice fed a high-fat diet. Collateral arteriogenesis, documented by $\alpha_v\beta_3$ SPECT imaging in the proximal hindlimb at a late time point, also was significantly impaired in mice fed a high-fat diet. This reflects a more global defect in endothelial function and inadequate NO-elaborating responses to additional growth factors important in arteriogenesis. The combined imaging approaches demonstrated a broad and sustained defect, over an extended period, in complementary fashion.

Ceramide has been shown to mediate insulin resistance in brown adipose tissue[35] and to negatively regulate insulin action in muscle by inhibiting Akt activity.[36] With the present study, we have demonstrated palmitate-induced ceramide production in primary ECs, and aortic ceramide generation in mice fed a high-fat diet, using LC-MS/MS to document the increase in early-species ceramide metabolites. The SPT inhibitor myriocin, an effective inhibitor of the first step in endogenous ceramide synthesis (ie, the formation of 3-ketosphinganine from serine and palmitoyl-CoA), largely prevented the inhibitory effect of PA on VEGF-induced eNOS phosphorylation and cord formation. Furthermore, using *Sptlc2*$^{-/+}$ mice, we demonstrated that high-fat diet-induced impairment of VEGF signaling and angiogenesis are largely dependent on *de novo* synthesis of ceramide. One caveat is that SPT inhibition would cause depletion of all sphingolipids. It is possible that, in addition to ceramide, sphingomyelin could be playing an inhibitory role. We found that the relatively specific sphingomyelin synthase 2 inhibitor D609 had a marginal effect (much less than myriocin) on PA-induced attenuation of VEGF-stimulated eNOS phosphorylation (data not shown). However, it remains possible that other sphingolipids play some role in this fatty acid–induced effect.

Because ceramide can activate PP2A, which in turn can dephosphorylate Akt, eNOS, and ERK,[36] we investigated PP2A involvement in EC resistance to VEGF after short-term exposure to PA. PP2A–eNOS association was enhanced in PA-treated ECs, promoting dephosphorylation and consequently reducing NO production. In a recent report by Zhang et al,[37] ceramide-induced association of PP2A with eNOS and Akt was implicated in vascular dysfunction and insulin resistance in obese mice, findings similar to some of our observations on the ceramide–PP2A–eNOS axis; however, several factors and findings make the present study sufficiently distinct. First, the much shorter duration of exposure of mice to a diet high in saturated fat (3 weeks in the present study, compared with 3 months in the study of Zhang et al[37]) suggests that ceramide-dependent PP2A-mediated VEGF resistance precedes obesity. Second, using much lower concentrations of PA (100 μmol/L versus 500 μmol/L) and myriocin (100 nmol/L versus 10 μmol/L), which are more physiologically relevant for PA and probably more specific for myriocin, we demonstrated effects of PA and myriocin on VEGF-induced Akt and ERK phosphorylation, whereas Zhang et al[37] indicated that *de novo* synthesized ceramide activates PP2A without affecting Akt, ERK, or AMPK activation after stimulation with insulin. Our present findings leave open the possibility that signaling downstream of VEGFR2 is more sensitive to inhibition by ceramide-induced PP2A.

In preliminary experiments, we observed that this induced signaling defect is not caused by all fatty acids; in particular, the polyunsaturated fatty acid eicosapentaenoic acid had no inhibitory effect (data not shown). This is consistent with previous studies demonstrating augmented insulin-stimulated NO production in cells pretreated with eicosapentaenoic acid.[38] A monosaturated prevalent fatty acid, oleic acid, also did not attenuate VEGF-induced signaling in our models (data not shown).

We have defined a mechanism by which FFAs, such as are elevated in metabolic syndrome, lead to endothelial insensitivity to a prototypic angiogenic growth factor, a defect that correlates with endothelial dysfunction. As already noted, we chose relatively low concentrations of PA and a model system in which we can segregate this ceramide-activated PP2A effect. We recognize that many other mechanisms could contribute to lipid-induced endothelial abnormalities. Palmitate treatment can lead to the reduction of key mitochondrial biogenesis regulators, including PGC-1α and cytochrome c oxidase subunit IV.[39] There are also potential links among ceramide, PKC, and insulin resistance. Ceramide has been shown to disable the Akt pleckstrin homology domain interaction with membrane phosphatidylinositol-3,4,5-trisphosphate by activation of PKC-ζ, which phosphorylates the Akt pleckstrin homology domain.[40] Because of this potential ceramide–PKC-ζ–Akt link, we investigated the activation and role of PKC-ζ in PA-induced inhibition of VEGF responses in BAEC. At the PA concentrations we used, there was minimal activation of PKC-ζ, and no reversal of the VEGF signaling abnormalities on effective PKC-ζ inhibition using a pseudosubstrate inhibitor (data not shown). Finally, although we focused on VEGF responses and emphasized vascular signaling initiated by prototypic angiogenic growth factors, the role of abnormal insulin signaling may, in and of itself, play a role in vascular pathology (as has been shown by others[41]).

Thus, although there are likely many molecular contributors to vascular disease in dysmetabolic states, here we have described an important and novel pathological pathway induced by a direct PA effect on the endothelium. Similar to insulin resistance in skeletal muscle and liver, this is a form of VEGF resistance at the level of the endothelium with diminished NO production and loss of growth factor-mediated cell survival signals. This resistance suggests a limited role for angiogenesis stimulation by simply increasing growth factor delivery in ischemic conditions, and likely explains the minimal success of VEGF trials in vascular disease.[42] The key role of ceramide in these VEGF signaling abnormalities raises the possibility that safe

pharmacological inhibitors of endogenous ceramide synthesis could promote maintenance of vascular homeostasis in dysmetabolic states. Myriocin has been shown to attenuate atherosclerosis in murine models[8] and, based on the present study, it would be a useful agent in early endothelial dysfunction studies. A potential application of these molecular studies is to direct preventive efforts toward maintaining normal endothelial function in metabolic syndrome.

## Acknowledgments

We thank GE Healthcare for providing the SPECT imaging agent and Dana Brenckle for assistance with manuscript preparation.

## Supplemental Data

Supplemental material for this article can be found at *http://dx.doi.org/10.1016/j.ajpath.2014.01.009*.

## References

1. Engler MM, Engler MB, Malloy MJ, Chiu EY, Schloetter MC, Paul SM, Stuehlinger M, Lin KY, Cooke JP, Morrow JD, Ridker PM, Rifai N, Miller E, Witztum JL, Mietus-Snyder M: Antioxidant vitamins C and E improve endothelial function in children with hyperlipidemia: Endothelial Assessment of Risk from Lipids in Youth (EARLY) trial. Circulation 2003, 108:1059−1063
2. Halcox JP, Schenke WH, Zalos G, Mincemoyer R, Prasad A, Waclawiw MA, Nour KR, Quyyumi AA: Prognostic value of coronary vascular endothelial dysfunction. Circulation 2002, 106:653−658
3. Steinberg HO, Tarshoby M, Monestel R, Hook G, Cronin J, Johnson A, Bayazeed B, Baron AD: Elevated circulating free fatty acid levels impair endothelium-dependent vasodilation. J Clin Invest 1997, 100:1230−1239
4. Steinberg HO, Chaker H, Leaming R, Johnson A, Brechtel G, Baron AD: Obesity/insulin resistance is associated with endothelial dysfunction. Implications for the syndrome of insulin resistance. J Clin Invest 1996, 97:2601−2610
5. Miyazawa-Hoshimoto S, Takahashi K, Bujo H, Hashimoto N, Saito Y: Elevated serum vascular endothelial growth factor is associated with visceral fat accumulation in human obese subjects. Diabetologia 2003, 46:1483−1488
6. Blann AD, Belgore FM, McCollum CN, Silverman S, Lip PL, Lip GY: Vascular endothelial growth factor and its receptor, Flt-1, in the plasma of patients with coronary or peripheral atherosclerosis, or type II diabetes. Clin Sci (Lond) 2002, 102:187−194
7. Belgore FM, Blann AD, Li-Saw-Hee FL, Beevers DG, Lip GY: Plasma levels of vascular endothelial growth factor and its soluble receptor (sFlt-1) in essential hypertension. Am J Cardiol 2001, 87: 805−807. A9
8. Hojjati MR, Li Z, Jiang XC: Serine palmitoyl-CoA transferase (SPT) deficiency and sphingolipid levels in mice. Biochim Biophys Acta 2005, 1737:44−51
9. Miles J, Glasscock R, Aikens J, Gerich J, Haymond MA: Microfluorometric method for the determination of free fatty acids in plasma. J Lipid Res 1983, 24:96−99
10. Kyriakides TR, Zhu YH, Yang Z, Huynh G, Bornstein P: Altered extracellular matrix remodeling and angiogenesis in sponge granulomas of thrombospondin 2-null mice. Am J Pathol 2001, 159: 1255−1262
11. Ackah E, Yu J, Zoellner S, Iwakiri Y, Skurk C, Shibata R, Ouchi N, Easton RM, Galasso G, Birnbaum MJ, Walsh K, Sessa WC: Akt1/-protein kinase Balpha is critical for ischemic and VEGF-mediated angiogenesis. J Clin Invest 2005, 115:2119−2127
12. Russell KS, Haynes MP, Sinha D, Clerisme E, Bender JR: Human vascular endothelial cells contain membrane binding sites for estradiol, which mediate rapid intracellular signaling. Proc Natl Acad Sci USA 2000, 97:5930−5935
13. Yu C, Chen Y, Cline GW, Zhang D, Zong H, Wang Y, Bergeron R, Kim JK, Cushman SW, Cooney GJ, Atcheson B, White MF, Kraegen EW, Shulman GI: Mechanism by which fatty acids inhibit insulin activation of insulin receptor substrate-1 (IRS-1)-associated phosphatidylinositol 3-kinase activity in muscle. J Biol Chem 2002, 277:50230−50236
14. Dobrucki LW, Dione DP, Kalinowski L, Dione D, Mendizabal M, Yu J, Papademetris X, Sessa WC, Sinusas AJ: Serial noninvasive targeted imaging of peripheral angiogenesis: validation and application of a semiautomated quantitative approach. J Nucl Med 2009, 50: 1356−1363
15. Ylä-Herttuala S, Rissanen TT, Vajanto I, Hartikainen J: Vascular endothelial growth factors: biology and current status of clinical applications in cardiovascular medicine. J Am Coll Cardiol 2007, 49: 1015−1026
16. Liu W, Akhand AA, Takeda K, Kawamoto Y, Itoigawa M, Kato M, Suzuki H, Ishikawa N, Nakashima I: Protein phosphatase 2A-linked and -unlinked caspase-dependent pathways for downregulation of Akt kinase triggered by 4-hydroxynonenal. Cell Death Differ 2003, 10:772−781
17. Andjelković M, Jakubowicz T, Cron P, Ming XF, Han JW, Hemmings BA: Activation and phosphorylation of a pleckstrin homology domain containing protein kinase (RAC-PK/PKB) promoted by serum and protein phosphatase inhibitors. Proc Natl Acad Sci USA 1996, 93:5699−5704
18. Michell BJ, Chen ZP, Tiganis T, Stapleton D, Katsis F, Power DA, Sim AT, Kemp BE: Coordinated control of endothelial nitric-oxide synthase phosphorylation by protein kinase C and the cAMP-dependent protein kinase. J Biol Chem 2001, 276:17625−17628
19. Holland WL, Brozinick JT, Wang LP, Hawkins ED, Sargent KM, Liu Y, Narra K, Hoehn KL, Knotts TA, Siesky A, Nelson DH, Karathanasis SK, Fontenot GK, Birnbaum MJ, Summers SA: Inhibition of ceramide synthesis ameliorates glucocorticoid-, saturated-fat-, and obesity-induced insulin resistance. Cell Metab 2007, 5:167−179
20. Dobrowsky RT, Kamibayashi C, Mumby MC, Hannun YA: Ceramide activates heterotrimeric protein phosphatase 2A. J Biol Chem 1993, 268:15523−15530
21. Verheij M, Bose R, Lin XH, Yao B, Jarvis WD, Grant S, Birrer MJ, Szabo E, Zon LI, Kyriakis JM, Haimovitz-Friedman A, Fuks Z, Kolesnick RN: Requirement for ceramide-initiated SAPK/JNK signalling in stress-induced apoptosis. Nature 1996, 380:75−79
22. Miyake Y, Kozutsumi Y, Nakamura S, Fujita T, Kawasaki T: Serine palmitoyltransferase is the primary target of a sphingosine-like immunosuppressant, ISP-1/myriocin. Biochem Biophys Res Commun 1995, 211:396−403
23. Chen JK, Lane WS, Schreiber SL: The identification of myriocin-binding proteins. Chem Biol 1999, 6:221−235
24. Vessby B: Dietary fat, fatty acid composition in plasma and the metabolic syndrome. Curr Opin Lipidol 2003, 14:15−19
25. Wahlberg E: Angiogenesis and arteriogenesis in limb ischemia. J Vasc Surg 2003, 38:198−203
26. Luo F, Wariaro D, Lundberg G, Blegen H, Wahlberg E: Vascular growth factor expression in a rat model of severe limb ischemia. J Surg Res 2002, 108:258−267
27. Edwards D, Jones P, Haramis H, Battle M, Lear R, Barnett DJ, Edwards C, Crawford H, Black A, Godden V: 99mTc-NC100692−a tracer for imaging vitronectin receptors associated with angiogenesis: a preclinical investigation. Nucl Med Biol 2008, 35:365−375
28. Hua J, Dobrucki LW, Sadeghi MM, Zhang J, Bourke BN, Cavaliere P, Song J, Chow C, Jahanshad N, van Royen N, Buschmann I, Madri JA,

Mendizabal M, Sinusas AJ: Noninvasive imaging of angiogenesis with a 99mTc-labeled peptide targeted at alphavbeta3 integrin after murine hindlimb ischemia. Circulation 2005, 111:3255–3260
29. Brooks PC, Montgomery AM, Rosenfeld M, Reisfeld RA, Hu T, Klier G, Cheresh DA: Integrin alpha v beta 3 antagonists promote tumor regression by inducing apoptosis of angiogenic blood vessels. Cell 1994, 79:1157–1164
30. Soldi R, Mitola S, Strasly M, Defilippi P, Tarone G, Bussolino F: Role of alphavbeta3 integrin in the activation of vascular endothelial growth factor receptor-2. EMBO J 1999, 18:882–892
31. Steinberg HO, Baron AD: Vascular function, insulin resistance and fatty acids. Diabetologia 2002, 45:623–634
32. Inoguchi T, Li P, Umeda F, Yu HY, Kakimoto M, Imamura M, Aoki T, Etoh T, Hashimoto T, Naruse M, Sano H, Utsumi H, Nawata H: High glucose level and free fatty acid stimulate reactive oxygen species production through protein kinase C–dependent activation of NAD(P)H oxidase in cultured vascular cells. Diabetes 2000, 49:1939–1945
33. Simons M: Angiogenesis, arteriogenesis, and diabetes: paradigm reassessed? J Am Coll Cardiol 2005, 46:835–837
34. Li Y, Hazarika S, Xie D, Pippen AM, Kontos CD, Annex BH: In mice with type 2 diabetes, a vascular endothelial growth factor (VEGF)-activating transcription factor modulates VEGF signaling and induces therapeutic angiogenesis after hindlimb ischemia. Diabetes 2007, 56: 656–665
35. Teruel T, Hernandez R, Lorenzo M: Ceramide mediates insulin resistance by tumor necrosis factor-alpha in brown adipocytes by maintaining Akt in an inactive dephosphorylated state. Diabetes 2001, 50:2563–2571
36. Stratford S, Hoehn KL, Liu F, Summers SA: Regulation of insulin action by ceramide: dual mechanisms linking ceramide accumulation to the inhibition of Akt/protein kinase B. J Biol Chem 2004, 279: 36608–36615
37. Zhang QJ, Holland WL, Wilson L, Tanner JM, Kearns D, Cahoon JM, Pettey D, Losee J, Duncan B, Gale D, Kowalski CA, Deeter N, Nichols A, Deesing M, Arrant C, Ruan T, Boehme C, McCamey DR, Rou J, Ambal K, Narra KK, Summers SA, Abel ED, Symons JD: Ceramide mediates vascular dysfunction in diet-induced obesity by PP2A-mediated dephosphorylation of the eNOS-Akt complex. Diabetes 2012, 61:1848–1859
38. Lynn MA, Rupnow HL, Kleinhenz DJ, Kanner WA, Dudley SC, Hart CM: Fatty acids differentially modulate insulin-stimulated endothelial nitric oxide production by an Akt-independent pathway. J Investig Med 2004, 52:129–136
39. Sutherland LN, Capozzi LC, Turchinsky NJ, Bell RC, Wright DC: Time course of high-fat diet-induced reductions in adipose tissue mitochondrial proteins: potential mechanisms and the relationship to glucose intolerance. Am J Physiol Endocrinol Metab 2008, 295:E1076–E1083
40. Powell DJ, Hajduch E, Kular G, Hundal HS: Ceramide disables 3-phosphoinositide binding to the pleckstrin homology domain of protein kinase B (PKB)/Akt by a PKCzeta-dependent mechanism. Mol Cell Biol 2003, 23:7794–7808
41. Kim F, Tysseling KA, Rice J, Pham M, Haji L, Gallis BM, Baas AS, Paramsothy P, Giachelli CM, Corson MA, Raines EW: Free fatty acid impairment of nitric oxide production in endothelial cells is mediated by IKKbeta. Arterioscler Thromb Vasc Biol 2005, 25:989–994
42. Freedman SB, Isner JM: Therapeutic angiogenesis for coronary artery disease. Ann Intern Med 2002, 136:54–71